Cancer Cell International

RESEARCH

Open Access

TTI-101 targets STAT3/c-Myc signaling pathway to suppress cervical cancer progression: an integrated experimental and computational analysis

Yi Li[1] and Yuyan Dong[2*]

Abstract

Background Cervical cancer (CC) is a significant global health concern, demanding the consideration of novel therapeutic strategies. The signal transducer and activator of transcription 3 (STAT3) pathway has been implicated in cancer progression and is a potential target for therapeutic intervention. This study aimed to explore the therapeutic potential of TTI-101, a small molecule STAT3 inhibitor, in CC and investigate its underlying mechanisms.

Methods Molecular docking studies and molecular dynamics simulations were performed to explore the binding interaction between TTI-101 and STAT3 and assess the stability of the STAT3-TTI-101 complex. Cell viability assays, wound healing assays, colony formation assays, flow cytometry analysis, and gene expression analysis were conducted. In vivo xenograft models were used to assess the antitumor efficacy of TTI-101.

Results The in silico analysis shows a stable binding interaction between TTI-101 and STAT3. TTI-101 treatment inhibits cell viability, clonogenic ability, and cell migration in CC cells. Furthermore, TTI-101 induces apoptosis and cell cycle arrest. Analysis of apoptosis-related markers demonstrated dysregulation of Bax, Bcl-2, and Caspase-3 upon TTI-101 treatment. Moreover, TTI-101 caused G2/M phase arrest accompanied by a decrease in CDK1 and Cyclin B1 at mRNA levels. In the xenograft model, TTI-101 significantly inhibited tumor growth without adverse effects on body weight.

Conclusion TTI-101 exhibited anticancer effects by targeting the STAT3/c-Myc signaling pathway, inducing cell cycle arrest, and promoting apoptosis in CC cells. These findings provide valuable insights into the development of novel therapeutic strategies for cervical cancer. Further investigation is warranted to validate the clinical application of TTI-101.

Keywords Cervical cancer, TTI-101, Signal transducer and activator of transcription 3 (STAT3), Cell cycle arrest, STAT3 inhibitor

*Correspondence:
Yuyan Dong
dyy20230102@126.com
Full list of author information is available at the end of the article

Graphical Abstract

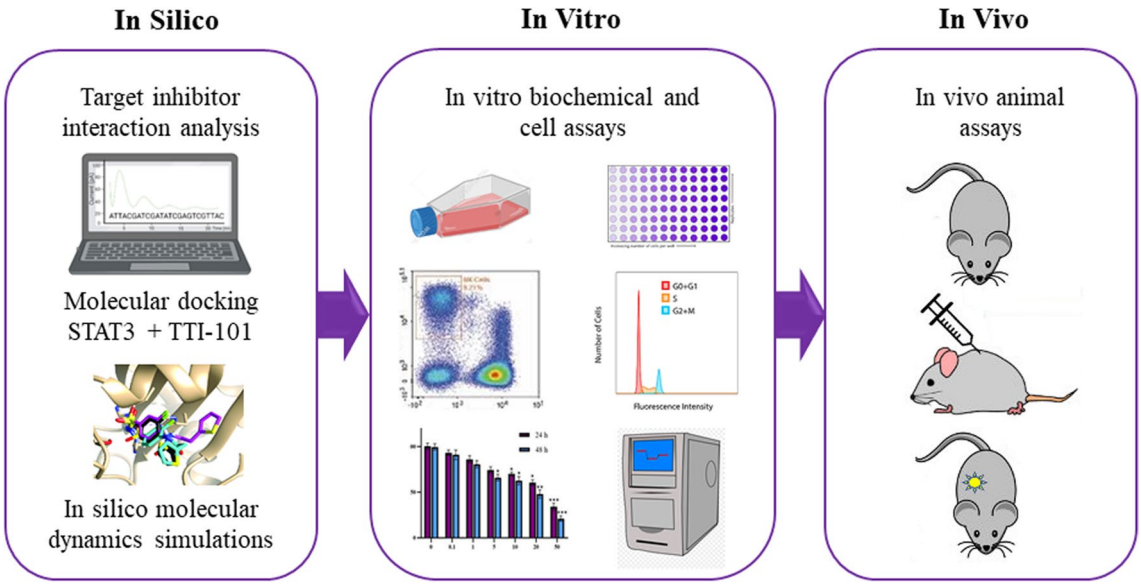

Introduction

Cervical cancer (CC) is the fourth most common cancer and second leading cause of cancer-related death among women in developing countries, with approximately 604,000 new cases and 342,000 deaths in 2020 [1]. Currently, surgery and radiotherapy are the main treatments for CC, but this disease has a high recurrence rate and drug resistance [2]. Therefore, studies on the pathophysiological mechanism of cervical cancer and the search for effective therapeutic agents are still crucial.

Cancer involves various signaling pathways, hence, the treatment should include molecules that target specific signaling pathways.

The signal transducer and activator of transcription (STAT) family proteins are a group of transcription factors that regulate gene expression related to the cell cycle, cell survival, and the immune response, and among them STAT3 is a well-known oncogene [3]. In normal cells, STAT3 was originally identified as a mediator of the acute phase of the inflammatory response under tight control [4]. Constitutive activation of STAT3 and its target genes stimulates cell-cycle progression, epithelial–mesenchymal transition, mediates immune evasion, and promotes inflammation, angiogenesis, and tumor invasion and metastasis, contributing to oncogenesis [5, 6].

The activation of receptor tyrosine kinases (RTKs) or Janus kinases (JAKs) can result in the phosphorylation of specific tyrosine residues on STAT3 (P-STAT3). This phosphorylation event leads to the formation of homo-dimers through the Src homology 2 (SH2) domains of STAT3. Subsequently, the P-STAT3 homodimers translocate into the nucleus where they regulate the transcription of target genes [4, 7]. Recent research suggests that an increased level of phosphorylated STAT3 (pStat3) is associated with a poor prognosis in various types of human cancers, including head and neck, lung, colorectal, gastric, breast, ovarian, cervical, and prostate cancers, as well as leukemia, lymphomas, and multiple myeloma [4, 8, 9]. Additionally, current studies have demonstrated that STAT3 also plays a significant role in the proliferation and apoptosis of cervical cancer cells. Specifically, STAT3 functions as a key oncogene by promoting cell proliferation and inhibiting apoptosis in these cells [10, 11].

STAT3 appears as an attractive therapeutic, therefore, several STAT3 inhibitors have been developed. STAT3 inhibitory strategies mainly focus on hindering the dimerization of STAT3 proteins by employing small molecules discovered through bioinformatics analysis [12, 13]. Consequently, extensive searches for compounds that target the STAT3 protein, particularly focusing on the interaction between the SH2 domain and the phosphorylated tyrosine residue, have yielded a multitude of synthetic small molecules. Notable among them are STA-21, Stattic, STX-0119, LLL12, BBI608, and OPB-31121, which exhibit remarkable potency [6, 14–19]. Additionally, other categories of inhibitors encompass peptides or peptide-memetic, natural products (e.g., resveratrol,

curcumin, and XYA-2), as well as oligodeoxynucleotide decoys and antisense oligonucleotides [20–22].

TTI-101 (formerly C188-9) is a small molecule STAT3 inhibitor that possesses several advantageous characteristics as a chemical genetics probe. It binds to STAT3 with high affinity ($Kd = 4.7$ nM) and effectively hinders its interaction with receptor-based pY-peptide ligands [23]. This prevents the activation and nuclear translocation of STAT3, thereby inhibiting its transcriptional activity. By interfering with STAT3-mediated signaling, TTI-101 disrupts the expression of genes regulated by STAT3, which are crucial for tumor cell survival and immune sequestration. Additionally, TTI-101 has been shown to selectively target canonical STAT3 functions while sparing non-canonical contributions, such as oxidative phosphorylation. This selectivity contributes to its favorable safety profile and reduces the potential for off-target or on-target toxicity [24]. Furthermore, this small molecule displays excellent oral bioavailability in various animal models and humans. Utilizing TTI-101 in preclinical studies has provided insights into the role of STAT3 across different tissues in human and rodent disease models, including cancer, chronic inflammatory diseases, and fibrotic diseases [25]. Pharmacology and toxicology assessments in rats and dogs were conducted over 28 days to determine the initial dose for human testing in cancer patients and enable a Phase 1 study of TTI-101 in patients with solid tumors. Due to its ability to target STAT3, TTI-101 has been studied in several cancers types and inflammatory diseases [13, 26]; however, its role in CC has not been reported.

Therefore, we conducted the present study to evaluate the effects and underlying mechanisms of TTI-101 in HeLa cervical cancer cells. To this end, we performed molecular docking and molecular dynamics analyses to explore the interaction between TTI-101 and STAT3. Moreover, in vitro and in vivo experiments were conducted to investigate the antitumor effects of TTI-101 on cervical cancer with constitutively activated STAT3 and the molecular mechanisms of action.

Materials and methods

Molecular docking

Molecular docking studies were performed using AutoDock vina to investigate the binding interaction between STAT3 protein and TTI-101 ligand [27]. The three-dimensional crystal structure of STAT3 was obtained from the RCSB Protein Data Bank (PDB ID: 6QHD). The TTI-101 ligand structure was retrieved from PubChem database (CID: 1,324,494) and prepared using Open Babel [28]. The protein structure was preprocessed by removing all water molecules, adding hydrogen atoms and assigning Gasteiger charges. The ligand structure was converted to PDBQT format. Grid boxes were centered on the binding site of the STAT3 protein with dimensions of $60 \times 60 \times 60$ points and 0.375 Å spacing. Docking calculations were performed using the Lamarckian Genetic Algorithm with 100 runs. The docked conformations were ranked according to binding energy, and the conformation with the lowest binding energy was selected for further analysis. Molecular graphics visualization and analysis of protein–ligand interactions were performed using Discovery Studio Visualizer [29].

Molecular dynamics simulations

Molecular dynamics (MD) simulations were carried out using GROMACS 2020.3 package to study the dynamic stability of the STAT3-TTI-101 complex [30]. The bound complex obtained from molecular docking was used as the starting structure. The force field parameters for the protein were taken from CHARMM36 force field, while the ligand topology was generated using the CGenFF server [31, 32]. The complex was solvated in a cubic box of TIP3P water molecules and neutralized by adding counter ions. Energy minimization was performed using the steepest descent algorithm until a tolerance of 1000 kJ/mol. Equilibration was done in two steps—first, a 100 ps position restrained NVT equilibration and then a 100 ps NPT equilibration at 300 K temperature and 1 bar pressure. The production MD run was performed for 100 ns timescale with a time step of 2 fs. The particle mesh Ewald (PME) method utilized for treating long-range electrostatic interactions. Temperature and pressure were maintained using the v-rescale thermostat and Parrinello-Rahman barostat respectively [33]. All bonds were constrained using the LINCS algorithm. Trajectory analysis was done using built-in GROMACS utilities.

Inhibitor

TTI-101 (C188-9) was purchased from MCE (Monmouth Junction, NJ, USA) and dissolved in sterile dimethyl sulfoxide (DMSO; Merck Millipore, Billerica, MA, USA). The stock solution was stored at − 20 ℃ until use. The final concentration of DMSO used as the vehicle control did not exceed 0.1%.

Cell culture

The human cervical cancer cell line HeLa was obtained from Shanghai Institute of Cell Biology of the Chinese Academy of Sciences and grown in RPMI-1640 medium containing 10% fetal bovine serum (FBS), 100 U/ml penicillin, and 100 μg/ml streptomycin (all reagents were obtained from Gibco, CA, USA). The cells were incubated at 37 ℃ in a saturated humidified atmosphere with 5% CO2.

Cell viability assay

Cell viability assays were carried out using the MTT [3-(4,5-dimethylthiazol-2-yl)-2,5-diphenyl tetrazolium bromide] assay [34]. HeLa cells were seeded in triplicate at a density of 1×10^4 cells/well in a 96-well plate with 200 µL/well of standard culture media and incubated until they reached 85% confluence. The cells were then treated with either 0.1% DMSO (control) or various concentrations of TTI-101 (0–50 µM) and incubated for 24 or 48 h at 37 ℃. After that, 20 µL/well MTT (5 g/L) solution was added to each well followed by incubation for 3 h at 37 ℃. The medium was then replaced with 100 µL of DMSO to dissolve the formed formazan crystal in each well. Finally, the absorbance of each well was measured using ELISA plate reader at 570 and 630 nm (Bio-Rad, USA), and IC50 values were calculated by Prism 8 (GraphPad Software).

Wound healing assay

The wound healing assay was performed to ascertain the migrate ability of cancer cells according to previously reported method [35]. HeLa cells were plated in a 12-well culture dish and grown until confluence. The cells were then scratched using a 200 µL sterile pipet tip, washed twice with aseptic PBS to remove debris and non-adherent cells. The cells were treated with TTI-101 (20 and 40 µM) in treatment group and DMSO in control group. The cells were allowed to migrate into the scratched area and observed under the microscope and photographed at different times (0 and 24 h). The percentage of wound healing was calculated using the formula: (% wound healing) = average of [(gap area: 0 h) − (gap area: 24 h)]/(gap area: 0 h) × 100.

Colony formation assay

HeLa cells were seeded in 6-well plates (2000 cells/well) and treated with DMSO or TTI-101 for 24 h, and then cultured with drug-free culture medium for 7 days. After a week, the cells were washed and fixed with paraformaldehyde for 15 min. After stained with 0.1% crystal violet for 10 min, the cells were rinsed, dried, and images captured under a phase-contrast microscope to quantify the number of colonies in each well. Data are presented as a percentage of colonies ± SD relative to untreated controls.

Flow cytometry analysis of cell cycle and apoptosis

The HeLa cells were cultured in completed RPMI medium in a T25 culture flask. After reaching 85% confluence, the culture medium was changed to DMSO or IC50 dose of TTI-101 (18.7 µM) for an additional 48 h. After the treatment, the cells were harvested, centrifuged at 1000 × *g* for 5 min at room temperature, and then washed twice with ice-cold PBS. These cells were used for cell cycle and apoptosis analysis. To investigate how cell cycle distribution is influenced by TTI-101, cells were fixed with 70% alcohol at 4 ℃ for overnight, then re-suspended in PI and 1% RNAase A solution for 30 min at 37 ℃C in the dark and analyzed using flow cytometry (BD Biosciences, San Jose, CA, USA). *FlowJo* software (v7.6.1, USA) was used to analyze the percentage of cells in each cell cycle phases.

Apoptotic cell death was detected using Annexin-V and propidium iodide (PI) staining, using the FITC Annexin V apoptosis detection kit (BD Biosciences, San Jose, CA, USA), according to the manufacturer's instructions. Briefly, the cell pellet was re-suspended in a binding buffer solution and incubated with Annexin-V FITC and PI solutions for 15 min. Then quantification of apoptosis of cells was analyzed using flow cytometry, and the acquisition data were interpreted using *FlowJo* software (v7.6.1, USA).

Gene expression by quantitative real-time-PCR

HeLa cells were seeded at 1×10^6 cells and grown for 24 h, then were treated with lethal concentrations of TTI-101 for 48 h. The gene expression levels of BAX, Bcl-2, Caspase 3 (CAS-3), CDK1, Cyclin B1, and c-Myc were determined in TTI-101-treated and untreated HeLa cells. After that, total RNA was extracted from cells using TRIzol (Invitrogen, Life Technologies). The concentrations of the RNA samples were measured using the nanodrop instrument. Then, the reverse transcription polymerase chain reaction (RT-PCR) experiment was set up with target genes, and the primer pairs listed in Table 1. The relative expression level of genes was calculated using the $2^{-\Delta\Delta Ct}$ method with GAPDH as an internal control [36].

Protein expression analysis

Western blot analysis was performed according to previously reported methods [37]. HeLa cells from the control and TTI-101 treated groups were rinsed in cold PBS. Total protein was extracted using the RIPA buffer (Beyotime, Shanghai, China) and its concentration determined using the bicinchoninic acid (BCA) assay. Cell lysate was resolved by SDS-PAGE and transferred to the PVDF membranes. The blots were probed with antibodies against Bcl-2, Bax, GAPDH (Santa Cruz Biotechnology, CA, USA), STAT3, p-STAT3 (Y705), survivin (Cell Signaling Technology), c-Myc and Cyclin B1 (Thermo Scientific, MA USA) followed by incubation in the corresponding horseradish peroxidase (HRP)-conjugated secondary antibody. Finally, protein bands were detected using chemiluminescence (ECL) kit and the relative protein expression was quantified using the software *ImageJ*.

Table 1 Primers for RT-qPCR analysis

Gene	Forward primer	Reverse primer
Bax	5′-GCGTCCACCAAGAAGCTGAG- 3′	5′-ACCACCCTGGTCTTGGATCC- 3′
Bcl2	5′-ATCGCCCTGTGGATGACTGAGT- 3′	5′-GCCAGGAGAAATCAAACAGAGGC- 3′
Caspase-3	5′-ACATGGAAGCGAATCAATGGACTC- 3′	5′-AAGGACTCAAATTCTGTTGCCACC- 3′
c-Myc	5′-CACAGCAAACCTCCTCACAG-3′	5′-GGTGCATTTTCGGTTGTTGC- 3′
CDK1	5′-GGGTCAGCTCGCTACTCAAC- 3′	5′ -AAGTTTTTGACGTGGGATGC- 3′
Cyclin B1	5′-GAAACATGAGAGCCATCCT- 3′	5′- TTCTGCATGAACCGATCAAT- 3′
GAPDH	5′-GTCTCCTCTGACTTCAACAGCG- 3′	5′-ACCACCCTGTTGCTGTAGCCAA- 3′

Mouse xenograft models

The animal experiment was approved by the Animal Experiment Ethics Committee of Shandong Provincial Third Hospital (AWE-2019-047). Female athymic nude mice, aged 4–5 weeks (weighing, 20–25 g), were purchased from Vital River Laboratory. HeLa cells (5×10^6 cells) in 200 μL PBS were injected subcutaneously into the right flank region of nude mice. When the tumor volume reached about 100 mm^3, the animals were divided into two groups (n = 6), randomly. Mice in the treatment group received TTI-101 (100 mg/kg, three times a week) for a duration of 3 weeks, while the control group received vehicle injections.

To assess the impact of STAT3 knockout on cervical cancer, the Human STAT3 knockout HeLa cell line (ab255436) was cultured in DMEM (High Glucose) supplemented with 10% FBS and 1% antibiotic medium and maintained at 37 ℃ in a humidified atmosphere with 5% CO2. Similar to the aforementioned procedure, STAT3 KO HeLa cells (5×10^6 cells) were injected into the nude mice (n = 6), and tumor growth was assessed in compared to the control group. Tumor volume was measured in all groups every 3 days using calipers and calculated using the formula: 0.5 (length × $width^2$) [38]. All mice were mercy sacrificed at the end of the research by cervical dislocation and tumors were harvested from them.

Statistical analysis

Student's unpaired t-test and One-way analysis of variance (ANOVA) followed by Tukey's posttest were used to analyze statistical significance between groups. A P-*value* < 0.05 was considered statistically significant. $^{*}P < 0.05$, $^{**}P < 0.01$ and $^{***}P < 0.001$ vs. the control group. Data are expressed as the means ± SD. GraphPad Prism (version 8.0; GraphPad Soft-ware) was used for all calculations.

Results

TTI-101 interaction with STAT3

Molecular docking was performed to investigate the binding mode of the TTI-101 ligand within the SH2 domain of STAT3. The best pose of TTI-101 achieved a binding energy of − 8.5 kcal/mol. Figure 1 shows the 2D interaction diagram with important contacts highlighted.

As shown in Table 2, TTI-101 formed two conventional hydrogen bonds with distances of 2.57 Å and 2.07 Å to the Gln63 and Ile634 residues, respectively. Additionally, TTI-101 engaged in pi-alkyl hydrophobic interactions with Lys591 at distances of 4.90 Å and 3.93 Å. Key interactions stabilizing the pose included the two hydrogen bonds and hydrophobic contacts with Lys591. These results provide insights into TTI-101's inhibitory mechanism against STAT3 through specific residue interactions. The computed binding mode, supported by interaction details from the table, offers a structural basis to guide development of analogous STAT3 inhibitors targeting this binding site.

Molecular dynamics analysis

MD simulation of the STAT3-TTI-101 complex revealed its stability and conformational changes. The RMSD analysis showed that the protein complex maintained a relatively low RMSD between 0.2 and 0.33 Å, indicating preservation of its structure and fold throughout the simulation (Fig. 2A). A slight initial increase in RMSD during the first 50 ns was followed by stabilization. The root-mean-square fluctuation (RMSF) analysis indicated overall limited flexibility, with most residues exhibiting RMSF values below 0.3 Å. However, residues 152–165 displayed higher fluctuations up to 0.5 Å, suggesting localized dynamics within the protein structure (Fig. 2B). No significant domain movements or subunit separation were observed, confirming the structural integrity of the protein complex during the simulation. The trajectories captured appropriate internal dynamics without disrupting the overall fold, validating the simulation's reliability for studying ligand binding mechanisms and conformational rearrangements. Analysis of protein–ligand interactions revealed intermittent hydrogen bonding throughout the simulation. Hydrogen bonds formed and broke quickly, with an average presence of 30–40% within each 10-s interval. Further analysis of longer time frames is needed

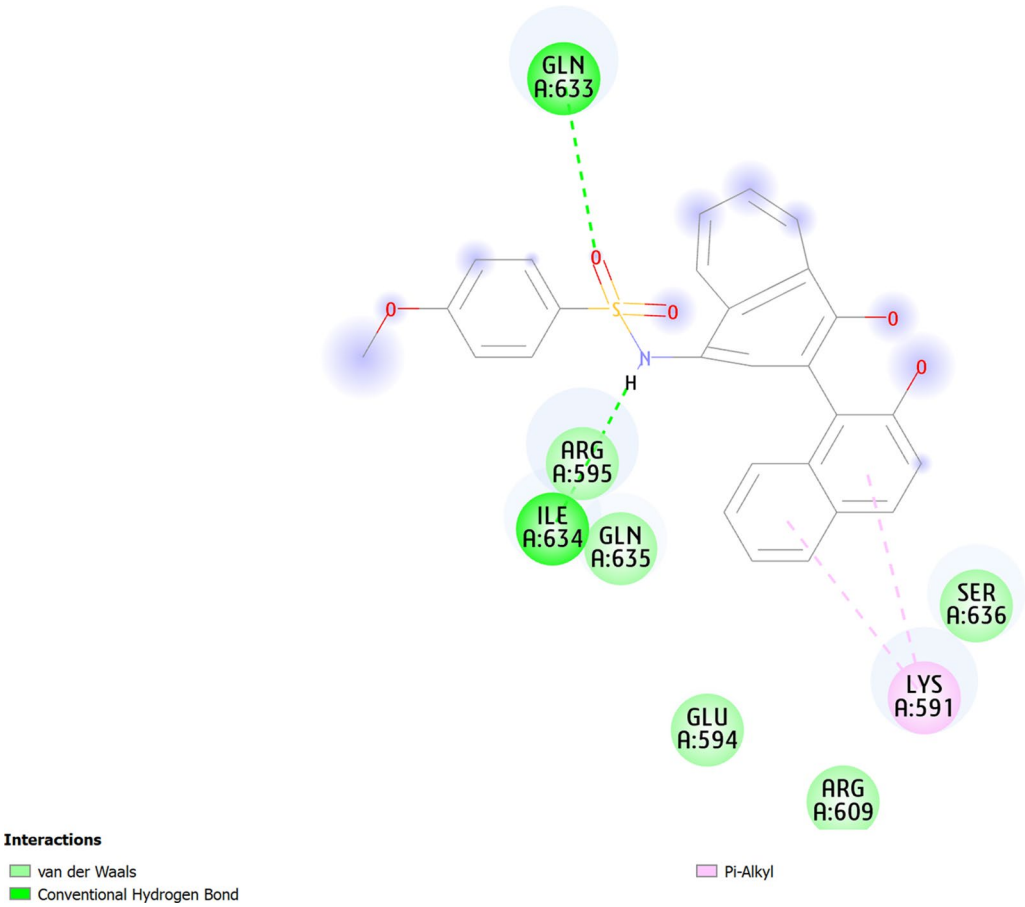

Fig. 1 2D interaction diagram highlighting key interactions between TTI-101 and STAT3 residues

Table 2 Key interactions between TTI-101 and STAT3 residues

Interactions	Distance	Category	Type
AGLN633—TTI-101	2.57	Hydrogen bond	Conventional hydrogen bond
TTI-101—ILE634	2.07	Hydrogen bond	Conventional hydrogen bond
TTI-101—LYS591	4.90	Hydrophobic	Pi-Alkyl
TTI-101—LYS591	3.93	Hydrophobic	Pi-Alkyl

to explore the stability and lifetimes of these non-covalent bonds (Fig. 2C).

TTI-101 decreases viability and clonogenic ability of cervical cancer cells

To test whether TTI-101 affects cell viability, we measured the proliferation of cervical cancer cells after 24 and 48 h treatments with TTI-101 by performing MTT assays. As shown in Fig. 3A, TTI-101 caused a dose- and time dependent reduction in cell viability of HeLa cells, which became significant at doses higher than 10 μM. After 24 h of treatment, the IC50 value of TTI-101 was 32.4 μM and further decreased to 18.7 μM after 48 h.

The percentage of colonies produced in clonogenic assays was measured to determine the effect of TTI-101 on the survival ability of cervical cancer cells. As illustrated in Fig. 3B. TTI-101 remarkably reduced the colony formation capacity in HeLa cervical cancer cell line to 44% compared to untreated control group.

TTI-101 suppresses cervical cancer cell migration

We then conducted wound healing assays to determine whether TTI-101 could inhibit cervical cancer cells

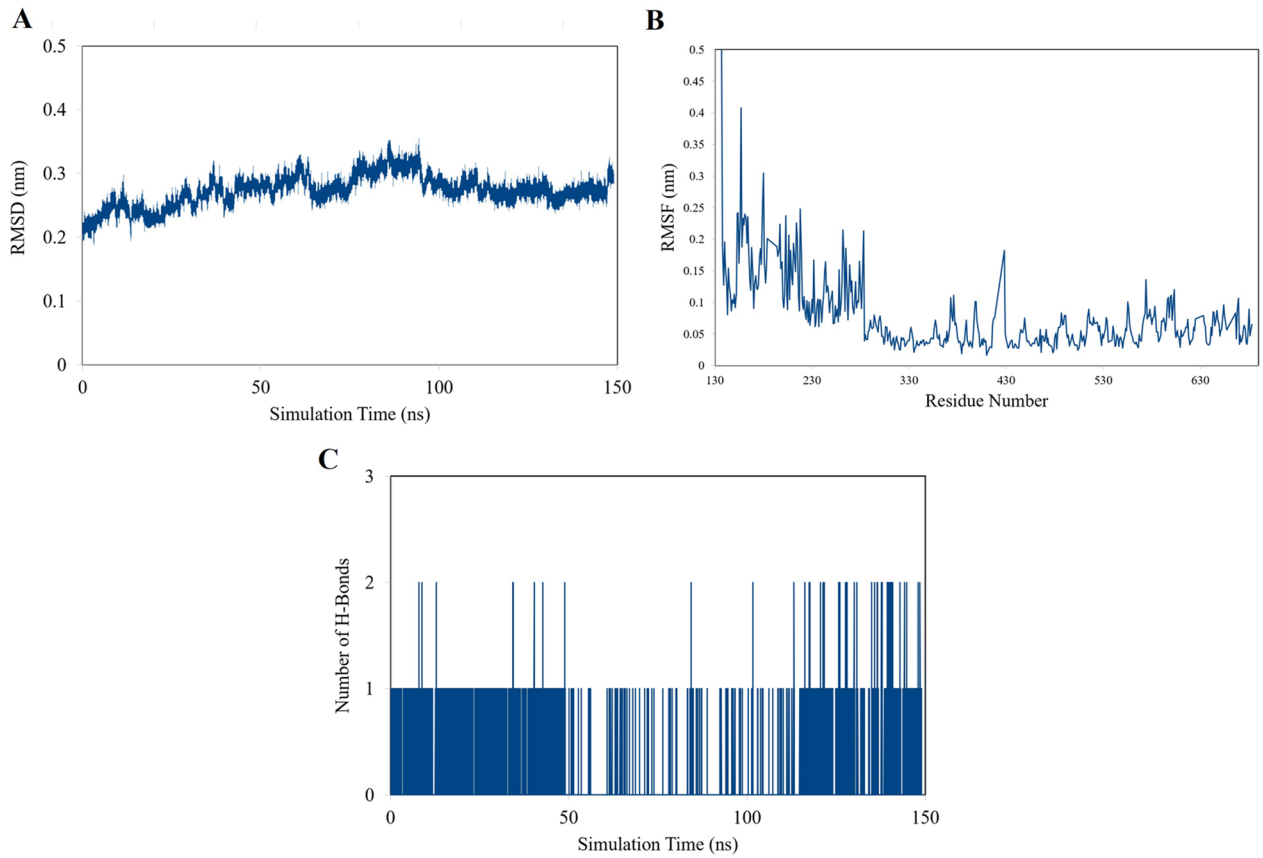

Fig. 2 **A** RMSD plot showing the stability of the STAT3-TTI-101 complex during the molecular dynamics simulation. **B** RMSF plot illustrating the fluctuation of residue positions within the protein complex during the simulation. **C** Hydrogen bonding frequency plot depicting the intermittent nature of protein–ligand interactions over time

migration. Our results showed that TTI-101 markedly inhibited the migratory ability of HeLa cells in a manner relying on concentration. The mean percentage of wound healing in the control group was 82% ± 3.4% that decreased to 25% ± 5.7% and 16% ± 1.8% at concentrations of 20 μM and 40 μM TTI-101, respectively (Fig. 3C).

TTI-101 induces apoptosis process and triggers G2/M cell cycle arrest

We then performed apoptosis analysis to better understand the mechanism involved in the antiproliferative activity of TTI-101. The apoptosis rate in the control group was 3.4 ± 0.06%. When the HeLa cells underwent treatment with TTI-101, the apoptosis rate considerably rose to 30.3 ± 0.14% (Fig. 4A). Meanwhile, the results of flow cytometry showed a significant increase in the number of cells in the G2/M phase and a decrease in the number of cells in the G0/G1 phase following TTI-101 treatment, while no significant difference was observed regarding the cell cycle distribution of HeLa cells in the S phases. As shown in Fig. 4B, the number of HeLa cells accumulated in the G2/M phase dramatically increased from 5.1 ± 0.16% in the control group to 12.5 ± 0.18% in the TTI-101-treated group and reduced from 42.7 ± 0.06% to 38.5 ± 0.1% in the G0/G1 phase 48 h after treatment. These results showed that the growth inhibition of HeLa cells was mediated by G2/M cell cycle arrest by TTI-101 and consequently STAT3 inhibition. To further validate this observation, we probed for key proteins and genes responsible for G2/M arrest and checked the expressions of Bax, bcl-2, c-Myc, Cyclin B1, and CDK1 genes.

TTI-101 changes the expression of apoptosis-related markers to induce apoptosis in HeLa cells

To understand the cytotoxicity mechanism of the TTI-101, we further checked the expression of the anti-apoptotic gene (Bcl-2) and Caspase-3, and one proapoptotic gene (Bax) after TTI-101 treatment by RT-PCR. We observed the efficient overexpression of the Bax (1.6 ± 0.09) and dysregulation of Bcl-2 (0.7 ± 0.1). Moreover, after treatment of HeLa cells with the IC50 value of

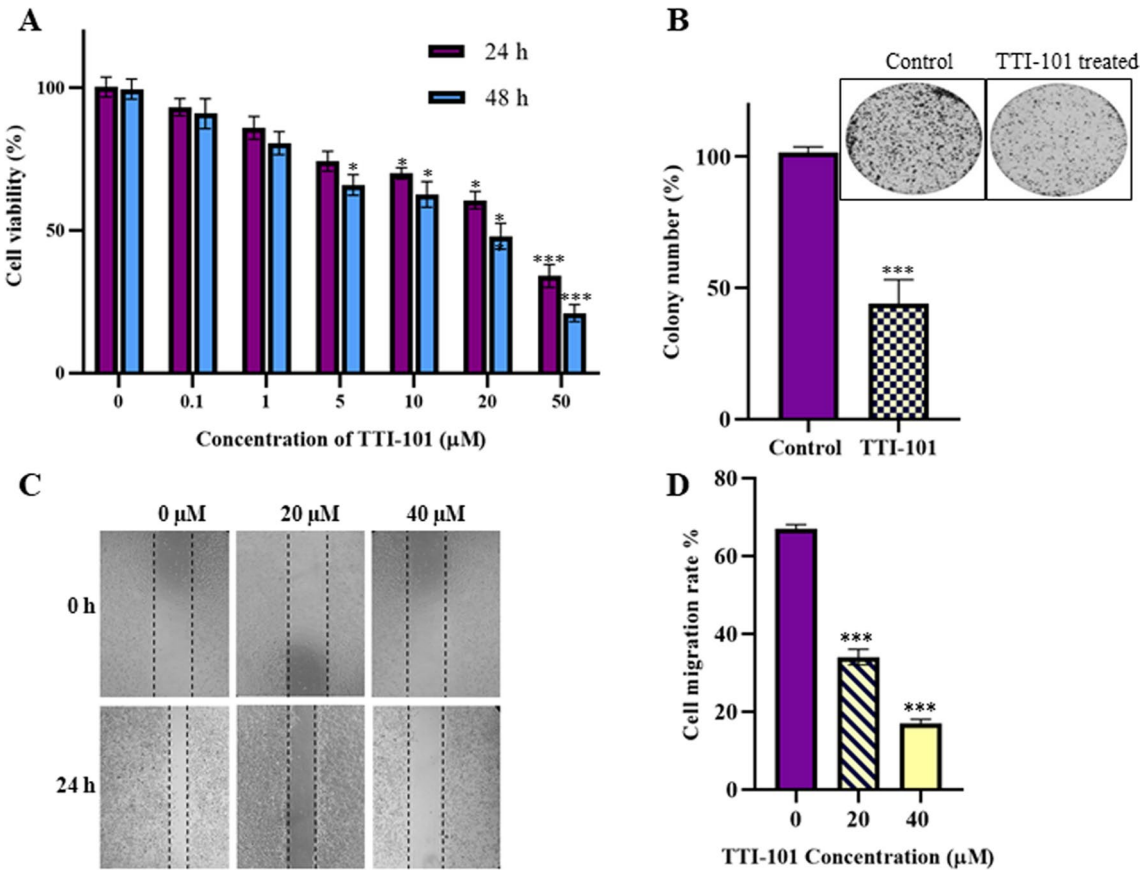

Fig. 3 **A** The inhibitory effect of TTI-101 on the viability of HeLa cell line. Cells were treated with indicated concentrations of TTI-101 for 24 and 48 h, and then subjected to an MTT assay. TTI-101impaired cell viability in a dose-and time-dependent manner compared with the control (untreated group). **B** The effect of TTI-101 on colony formation of HeLa cells. TTI-101 inhibited colony formation of these cells, significantly. **C** The effect of TTI-101 on migration of HeLa cells. Representative images from the wound healing assay of HeLa cells treated with TTI-101 at 0, 20, and 40 μM concentrations. **D** Data values are presented as a percentage of migration variation between starting (0 h) and ending (24 h) time points. Wound healing assay showing significant inhibition of cell migration after 24 h of exposure to TTI-101. All experiments were performed in triplicate and every independent experiment was performed three times. Data are represented as mean ± SD (n = 3), * $P < 0.05$; * * $P < 0.01$; * ** $P < 0.001$

TTI-101, the mRNA expression level of Caspase-3 significantly increased, while the expression level of c-Myc markedly decreased. The obtained expressions were normalized to the reference gene GAPDH, and Log2 values were taken to determine the fold changes in expression (Fig. 4C).

Effect of TTI-101 on STAT3 target genes expression and STAT3 phosphorylation

To investigate the molecular mechanism of anti-proliferation and cell cycle arrest of TTI-101 in HeLa cells, the effect of TTI-101 on the STAT3 target gene expression was analyzed. As shown in Fig. 4C, the expression of cyclin B1 and c-Myc genes were obviously decreased in response to TTI-101 compared with the control group. Consistent with the above results, western blotting results demonstrated that following TTI-101 treatment, the protein levels of survivin, cyclin B1, c-Myc, and Bcl-2 in HeLa cells were obviously decreased, whereas the expression level of Bax was increased (Fig. 5A, B). Moreover, the expression level of STAT3 and p-STAT3 was significantly downregulated in TTI-101-treatead cells (Fig. 5C, D).

We found that TTI-101 inhibited expression of the oncogene c-Myc through STAT3 in HeLa cells. These data indicated that TTI-101 suppresses cell proliferation and promotes cell cycle arrest in HeLa cells via inhibiting the STAT3 pathway and reducing the expression of its downstream target genes.

TTI-101 significantly inhibited tumor growth in vivo

Next, to test whether TTI-101 had an impact on cervical tumors in vivo, subcutaneous tumor growth xenograft models using HeLa was established. After 3 weeks

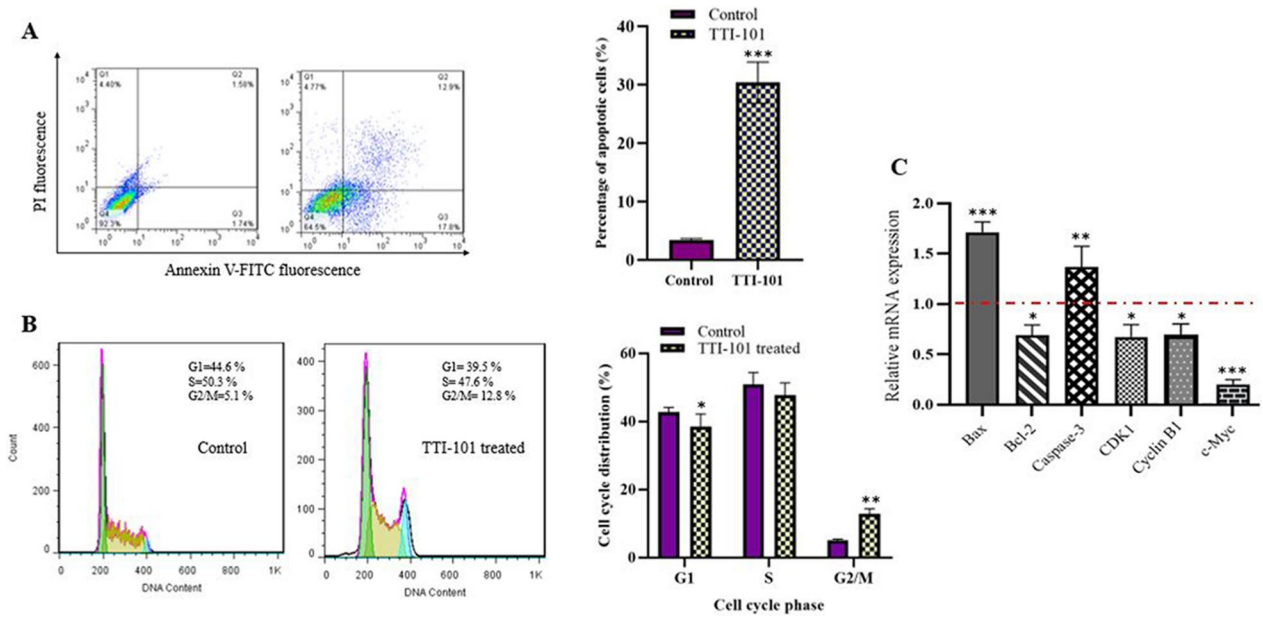

Fig. 4 Cell cycle distribution and apoptosis analysis of HeLa cells after treatment with IC50 dose of TTI-101. **A** The percentage of apoptotic cells (Q2 + Q3) in treated group was significantly higher than control group (30.3 ± 0.14% vs 3.4 ± 0.06%). **B** Increased percentage of G2/M-phase cells could be easily recognized (from 5.1 ± 0.16% to 12.5 ± 0.18%). The percentage of cells was measured using flow cytometry. **C** The Effects of TTI-101 on the expression of Bax, Bcl-2, Caspase 3, CDK1, Cyclin B1, and c-Myc in HeLa Cells. The experiments were performed in triplicate. *$p < 0.05$. **$P < 0.01$, ***$P < 0.001$ vs. the control group

of treatment, tumor volume in the vehicle control group and TTI-101 treated group were determined (Fig. 5E). According to Fig. 5F, TTI-101 significantly reduced tumor growth, while no significant difference in the mice's body weight was observed (Fig. 5G).

To further investigate the role of STAT3 in cervical cancer, STAT3 knockout HeLa cells were injected into nude mice to study the impact of STAT3 deficiency on tumor growth compared to TTI-101 treatment. As expected, the tumor growth in the STAT3 knockout group was significantly decreased compared to the control group, and it was even lower than that in the TTI-101 treated group (Fig. 5E). Specifically, the tumor volume in the STAT3 knockout group measured 233 ± 58.6 mm3, compared to 406.6 ± 70.3 mm3 in the TTI-101 treated group and 680.4 ± 106 mm3 in the vehicle control group (Fig. 5F). This finding suggests that the genetically inhibition of STAT3 have a greater impact on reducing cervical tumor growth than treatment with TTI-101.

Discussion

STAT3, a transcription factor with important roles in oncogenesis and cancer progression, is activated, phosphorylated, dimerized, and subsequently translocated into the nucleus in response to cytokines, growth factors, and other extracellular signals [39, 40]. Upon binding to sequence-specific DNA elements known as STAT3 response elements (SREs), p-STAT3 acts as a transcription factor, modulating the expression of numerous downstream target genes crucial for tumor growth and progression, such as cyclin B1, c-Myc, Bcl-xl, and Bcl-2 [6, 41, 42]. The significant involvement of STAT3 in cancer progression and tumorigenesis makes it a compelling molecular target for cancer therapy. A plethora of studies has shown demonstrated abnormal upregulation of STAT3 in various tumors, including cervical cancer [10, 43]. Until now, numerous small-molecule inhibitors have been developed to specifically target the SH2 domain of STAT3, crucial for STAT3 dimerization, resulting in reduced tumor cell viability, proliferation, and induction of apoptosis [44–47].

TTI-101 (c188-9) was discovered as a specific inhibitor targeting the phosphotyrosine peptide-binding site within the STAT3 SH2 domain with high affinity. Recent studies have increasingly focused on the potential of TTI-101 as an anti-tumor agent [48]. Experimental studies have revealed that TTI-101 enhances the therapeutic effectiveness of 5-Aza-2′-deoxycytidine (DAC) against pancreatic cancer through its regulation of demethylation [49]. Additionally, TTI-101 treatment demonstrated inhibition of hepatocellular carcinoma growth and protection of liver function in mice with hepatocyte-specific Pten deficiency [50]. Currently, several phase I/II clinical trial (e.g., NCT05440708, NCT05671835 and

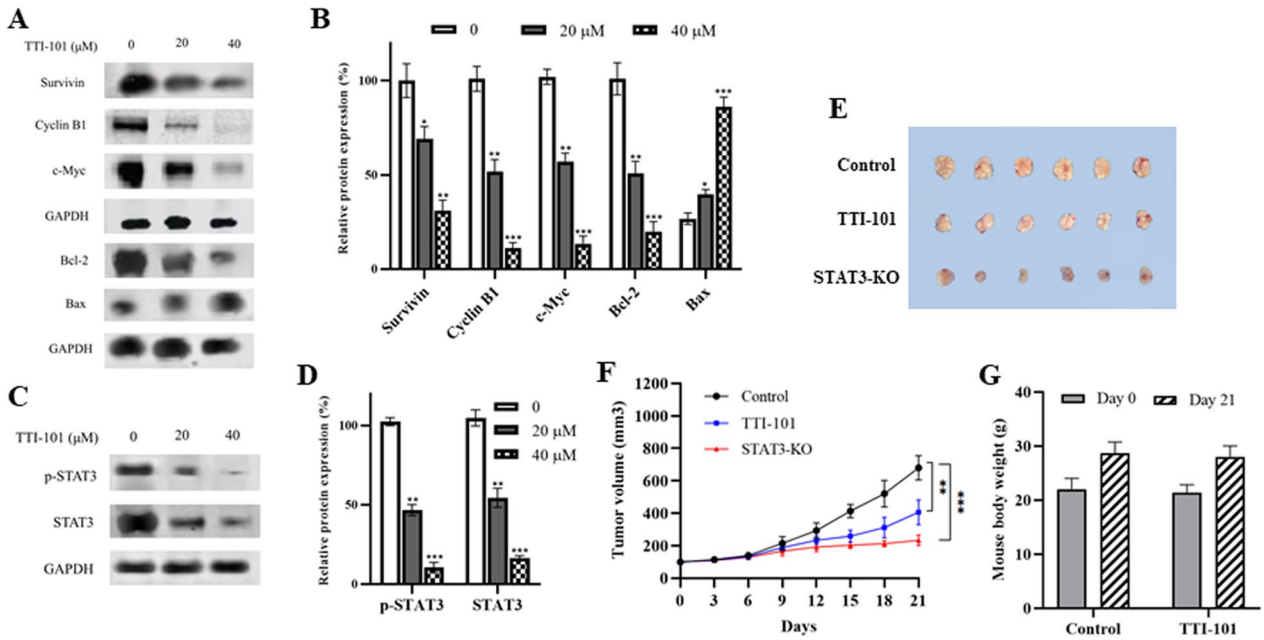

Fig. 5 **A**–**D** The effects of TTI-101 on the expression of STAT3 and its target genes in HeLa Cells. **A** The representative changes of Survivin, Cyclin B1, c-Myc, Bcl-2, and Bax expressions after treatment with different doses of TTI-101 for 48 h by western blot analysis. **B** Quantitative analysis for these protein levels in Hela cells. **C** The representative changes of p-STAT3 and STAT3 expressions after treatment with different doses of TTI-101 for 48 h by western blot analysis. **D** Quantitative analysis for these protein levels in Hela cells, GAPDH serves as a loading control in the western blot assay. **E**–**G** In vivo TTI-101 treatment and STAT3 knockout. **E** Photographs of tumors taken from different groups of mice after 3 weeks. **F** TTI-101 and STAT3 KO suppressed cervical tumor growth in the xenograft mouse model. The inhibition effect of STAT3 deletion was higher than TTI-101. The tumor volume of mice was monitored as a marker for tumor growth. **G** The body weights of xenograft mouse model of cervical cancer with TTI-101 treatment. No significant difference was observed in the body weight of the mice between the treatment and control groups. Results obtained from three independent experiments are expressed as means ± SD; **P* < *0.05*, ***P* < *0.01*, ****P* < *0.001* vs. the control group

NCT05384119) have been launched to assess the safety and efficacy of TTI-101 in cancer patients. In a phase I clinical study (NCT03195699), TTI-101 demonstrated good tolerability in patients with solid tumors, with no severe side effects observed. Encouragingly, this treatment elicited an antitumor response, with 13% of patients showing partial responses and 41% experiencing stable disease. Particularly positive outcomes were noted in hepatocellular carcinoma (HCC), where 20% of patients achieved a partial response. Building on these promising results, Phase 2 studies are currently underway to further investigate the efficacy of TTI-101 in patients with HCC and metastatic breast cancer [51]. Subsequently, we conducted a comprehensive investigation into the anticancer effects of TTI-101 on cervical cancer through a multifaceted approach encompassing in vitro and in vivo experiments, alongside molecular docking analysis.

Initially, utilizing molecular docking techniques, we elucidated a plausible binding mode of TTI-101 within the STAT3 SH2 domain, involving key interactions such as hydrogen bonds and pi-alkyl contacts. Molecular dynamics simulations validated the structural integrity of the STAT3-TTI-101 complex, exhibiting appropriate internal dynamics. Analysis of protein–ligand interactions provided insights into the intermittent nature of hydrogen bonding interactions between TTI-101 and STAT3 residues.

Subsequent in vitro experiments confirmed the inhibitory effects of TTI-101 on the viability, proliferation, and clonogenic ability of cervical cancer cells. MTT assay results revealed a dose- and time-dependent reduction in cell viability of HeLa cells following treatment with TTI-101. The IC50 value of TTI-101 decreased from 32.4 μM after 24 h of treatment to 18.7 μM after 48 h. Moreover, clonogenic assays demonstrated a notable decrease in the colony formation capacity of TTI-101-treated HeLa cells compared to the untreated control group.

In vivo studies have highlighted that STAT3 knockdown diminishes tumor growth and metastatic potential, underscoring the essential role of STAT3 activation in cancer progression and metastasis [52, 53]. Cervical cancer, known for its invasive and metastatic properties, poses challenges, making it imperative to explore compounds that suppress migration. Thus, we evaluated the effect of TTI-101 on cervical cancer cell migration through wound healing assays.

Our results revealed that TTI-101, along with its antiproliferative properties, exhibited substantial anti-migratory activity in HeLa cells in a concentration-dependent fashion. The percentage of wound healing significantly decreased at TTI-101 concentrations of 20 μM and 40 μM, illustrating its efficacy in curtailing migration compared to the control group.

To gain insights into the mechanisms underlying the antiproliferative activity of TTI-101, we performed apoptosis analysis and cell cycle distribution assays. Our results indicated that TTI-101 treatment significantly increased the apoptosis rate in HeLa cells compared to the control group.

In line with these findings, there was a noteworthy decrease in Bcl-2 expression at both the gene and protein levels, accompanied by an increase in Bax and Caspase-3 levels. These genes are pivotal in apoptosis, with Bax and Caspase-3 promoting cell death, while Bcl-2 acts as an inhibitor of apoptosis [54, 55].

In the present project, we verified that the cell cycle in TTI-101-treated HeLa cells was arrested at the G2/M phase (Fig. 4B). Proper cell cycle regulation is pivotal in preventing uncontrolled cell growth and proliferation [56]. The cell cycle checkpoint serves as a crucial regulatory point in controlling the progression of the cell cycle. It acts as a gatekeeper, allowing the cell to proceed to the next phase of the cycle only after successfully passing the checkpoint examination. Disrupted control of the cell cycle is a significant factor in the development of tumors. One significant regulatory factor in governing the checkpoint process is the CDK1/cyclin B complex [57]. At the end of the S phase, the activated CDK1/cyclin B complex triggers entry into mitosis [58]. Our findings indicate that following TTI-101 treatment, the expression levels of STAT3 and its target genes, including survivin, CDK1, cyclin B1, and c-Myc were notably reduced in HeLa cells.

Survivin is typically undetectable in most adult tissues, but its expression is significantly upregulated in a wide range of cancers [59]. It is cell cycle-regulated, with peak expression during the G2/M phase and lower levels during the G1 phase [60]. c-Myc is another STAT3 downstream gene that plays a crucial role in regulating CDK1/cyclin B1-dependent G2/M cell cycle progression [61, 62].

We speculated that inducing cell cycle arrest by targeting cell checkpoints and the STAT3 pathway may be another mechanism through which TTI-101 combats cervical cancer cells.

Finally, to validate the relevance of our findings in a physiologically relevant setting, we conducted in vivo experiments using a well-established subcutaneous cervical cancer xenograft models. It is worth noting that

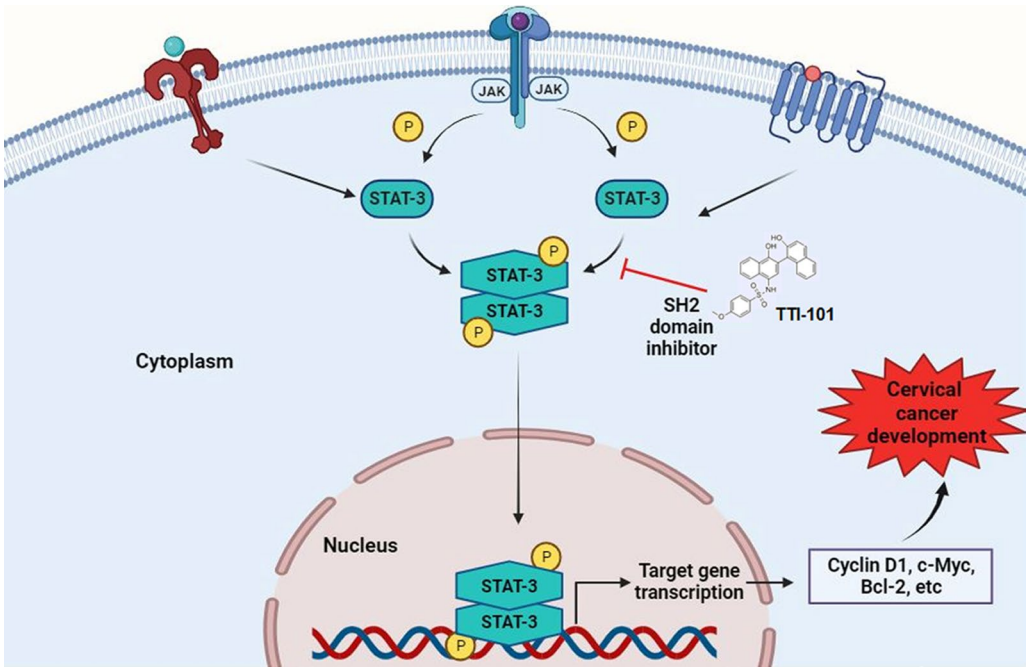

Fig. 6 Schematic illustration of the anti-tumor activity of TTI-101 on human cervical cancer cells by inhibiting the activity of STAT3/c-Myc signaling. Persistent STAT3 activation resulting from the activation of upstream growth factor receptors (e.g., IL-6 receptor), leads to abnormal proliferation and tumorigenesis in these cells. TTI-101 inhibits cell proliferation and promotes apoptosis through STAT3 downstream target genes in human CC cells

the concentrations of TTI-101 utilized in this study were selected based on prior research [24, 49, 63]. For instance, Kong et al. reported that TTI-101 (100 mg/kg) can augment the anti-metastasis effect of DAC in mouse pancreatic cancer models by inhibiting EMT [49]. In addition, Bharadwaj et al. showed that there were no observed clinical, anatomical, histological, or laboratory abnormalities in rats when they administered daily doses of up to 200 mg/kg/day for a duration of 28 days [24]. Thus, in present study, TTI-101 was tested on cervical cancer model in 100 mg/kg concentration. Consistent with previous studies, our results demonstrated that TTI-101 noticeably hindered tumor growth compared to the vehicle control group, indicating its potent antitumor efficacy. Notably, the treatment with TTI-101 did not result in significant changes in body weight, showing its potential as a well-tolerated therapeutic option for cervical cancer.

We also found that STAT3 knockout significantly inhibited the tumor growth in xenograph animal model. These observations highlight the potential efficacy of targeting STAT3 as a therapeutic strategy for cervical tumors, warranting further investigation into the underlying mechanisms of STAT3 inhibition in tumor suppression.

The docking results, corroborating the direct binding of TTI-101 to STAT3, align with our experimental findings, highlighting the anticancer effects of TTI-101 in cervical cancer through STAT3/c-Myc signaling inhibition (Fig. 6). The results emphasized that TTI-101 has the ability to modulate multiple intracellular pathways involved in cellular proliferation, apoptosis, and migration. This underscores TTI-101 as a promising therapeutic candidate and emphasizes the significance of targeting STAT3 in cervical cancer treatment.

The lack of direct comparison data between cancer and normal cells is a limitation of the current study. Ideally, future studies should include the evaluation of TTI-101's effects on normal cervical epithelial cells to further demonstrate the therapeutic window and selectivity of this compound. However, we can discuss the potential selectivity of TTI-101 based on the in vivo xenograft experiments performed. In these studies, we did not observe any significant adverse effects on the body weight of the mice treated with TTI-101. This suggests that the compound may have a preferential cytotoxic effect on the tumor cells without causing major systemic toxicity.

Conclusion

In summary, this study has confirmed the critical role of STAT3 in the progression of cervical cancer and highlighted the capacity of TTI-101 in the treatment of the disease. It was found that TTI-101 exerts anticancer functions by specifically targeting STAT3. The combination of in vitro and in vivo experiments, along with the molecular docking analysis, suggests the potential of TTI-101 as a promising therapeutic agent for cervical cancer treatment. Our results show that the inhibition of STAT3 by TTI-101 leads to the downregulation of c-Myc expression. The reduced c-Myc levels then impact the expression of cell cycle regulatory proteins, such as CDK1 and Cyclin B1, thereby inducing G2/M cell cycle arrest. Additionally, the suppression of the STAT3/c-Myc axis leads to the dysregulation of apoptosis-related proteins, including the upregulation of the pro-apoptotic Bax and the downregulation of the anti-apoptotic Bcl-2, ultimately promoting apoptosis in the cervical cancer cells. These findings pave the way for future investigations to evaluate the clinical potential of TTI-101 or explore its synergistic effects in combination with other anticancer agents for the treatment of cervical cancer.

Author contributions

YL: Investigation, Software, Formal analysis, writing—original draft preparation, Writing—review & editing. YD: Conceptualization, Methodology, Investigation, Supervision, Project administration, Validation, writing—original draft preparation, writing—review & editing; All authors read and approved the final manuscript.

Funding

This study is supported by Shandong Medical and Health Science and Technology Development Plan Project (2018WS283).

Data availability

The data that support the findings of this study are available from the corresponding author. No datasets were generated or analysed during the current study.

Declarations

Competing interests

The authors declare that they have no competing interest

Author details

[1]Department of Gynaecology, Shandong Provincial Third Hospital, Shandong University, No.11 Wuyingshan Middle Road, Tianqiao District, Jinan 250031, Shandong, People's Republic of China. [2]Department of Gynaecology, Shandong Provincial Maternal and Child Health Care Hospital, 238 Jingshi East Road, Jinan 250014, Shandong, People's Republic of China.

Received: 11 January 2024 Accepted: 29 July 2024
Published online: 12 August 2024

References

1. Mekuria M, et al. Prevalence of cervical cancer and associated factors among women attended cervical cancer screening center at Gahandi Memorial Hospital Ethiopia. Cancer Inf. 2021;20:11769351211068432.
2. Razlog R, Kruger CA, Abrahamse H. Enhancement of conventional and photodynamic therapy for treatment of cervical cancer with cannabidiol. Integr Cancer Ther. 2022;21:15347354221092706.
3. Subramaniam A, et al. Potential role of signal transducer and activator of transcription (STAT) 3 signaling pathway in inflammation, survival, proliferation and invasion of hepatocellular carcinoma. Biochim et Biophys Acta (BBA) Rev Cancer. 2013;1835(1):46–60.

4. Siveen KS, et al. Targeting the STAT3 signaling pathway in cancer: role of synthetic and natural inhibitors. Biochim et Biophys Acta (BBA) Rev Cancer. 2014;1845(2):136–54.
5. Avalle L, et al. STAT1 and STAT3 in tumorigenesis: a matter of balance. Jak-stat. 2012;1(2):65–72.
6. Zhao C, et al. A novel small molecule STAT3 inhibitor, LY5, inhibits cell viability, colony formation, and migration of colon and liver cancer cells. Oncotarget. 2016;7(11):12917.
7. Mengie Ayele T, et al. Role of JAK2/STAT3 signaling pathway in the tumorigenesis, chemotherapy resistance, and treatment of solid tumors: a systemic review. J Inflamm Res. 2022;15:1349–64.
8. Johnson DE, O'Keefe RA, Grandis JR. Targeting the IL-6/JAK/STAT3 signalling axis in cancer. Nat Rev Clin Oncol. 2018;15(4):234–48.
9. Al Zaid Siddiquee K, Turkson J. STAT3 as a target for inducing apoptosis in solid and hematological tumors. Cell Res. 2008;18(2):254–67.
10. De Arellano AR, et al. STAT3 activation is required for the antiapoptotic effects of prolactin in cervical cancer cells. Cancer Cell Int. 2015;15:1–8.
11. Morgan EL, Macdonald A. JAK2 inhibition impairs proliferation and sensitises cervical cancer cells to cisplatin-induced cell death. Cancers. 2019;11(12):1934.
12. Liu L, et al. Identification of a natural product-like STAT3 dimerization inhibitor by structure-based virtual screening. Cell Death Dis. 2014;5(6):e1293–e1293.
13. Song H, et al. A low-molecular-weight compound discovered through virtual database screening inhibits Stat3 function in breast cancer cells. Proc Natl Acad Sci. 2005;102(13):4700–5.
14. Beebe JD, Liu J-Y, Zhang J-T. Two decades of research in discovery of anticancer drugs targeting STAT3, how close are we? Pharmacol Ther. 2018;191:74–91.
15. Shih P-C, Mei K-C. Role of STAT3 signaling transduction pathways in cancer stem cell-associated chemoresistance. Drug Discov Today. 2021;26(6):1450–8.
16. Pan Y, et al. Stat3 inhibitor Stattic exhibits potent antitumor activity and induces chemo-and radio-sensitivity in nasopharyngeal carcinoma. PLoS ONE. 2013;8(1): e54565.
17. Rath KS, et al. HO-3867, a safe STAT3 inhibitor, is selectively cytotoxic to ovarian cancer. Can Res. 2014;74(8):2316–27.
18. Zuo M, et al. LLL12, a novel small inhibitor targeting STAT3 for hepatocellular carcinoma therapy. Oncotarget. 2015;6(13):10940.
19. Chen J, et al. STAT3 inhibitor BBI608 reduces patient-specific primary cell viability of cervical and endometrial cancer at a clinical-relevant concentration. Clin Transl Oncol. 2023;25(3):662–72.
20. Plens-Gałąska M, et al. SINBAD, structural, experimental and clinical characterization of STAT inhibitors and their potential applications. Sci Data. 2022;9(1):139.
21. Wiciński M, et al. Beneficial effects of resveratrol administration—Focus on potential biochemical mechanisms in cardiovascular conditions. Nutrients. 2018;10(11):1813.
22. Guan X, et al. Dual inhibition of MYC and SLC39A10 by a novel natural product STAT3 inhibitor derived from Chaetomium globosum suppresses tumor growth and metastasis in gastric cancer. Pharmacol Res. 2023;189:106703.
23. Xu X, et al. Chemical probes that competitively and selectively inhibit Stat3 activation. PLoS ONE. 2009;4(3): e4783.
24. Bharadwaj U, et al. Small-molecule inhibition of STAT3 in radioresistant head and neck squamous cell carcinoma. Oncotarget. 2016;7(18):26307.
25. Tweardy DJ. Drugging "undruggable" disease-causing proteins: focus on signal transducer and activator of transcription (Stat) 3. Trans Am Clin Climatol Assoc. 2022;132:61.
26. Park JS, et al. STA-21, a promising STAT-3 inhibitor that reciprocally regulates Th17 and Treg cells, inhibits osteoclastogenesis in mice and humans and alleviates autoimmune inflammation in an experimental model of rheumatoid arthritis. Arthritis Rheumatol. 2014;66(4):918–29.
27. Trott O, Olson AJ. AutoDock Vina: Improving the speed and accuracy of docking with a new scoring function, efficient optimization, and multithreading. J Comput Chem. 2010;31:455–61. https://doi.org/10.1002/jcc.21334.
28. O'Boyle NM, et al. Open babel: an open chemical toolbox. J Cheminf. 2011;3, 33. DOI: https://doi. org/10.1186/1758-2946-3-33.
29. Biovia DS. Discovery studio modeling environment. San Diego: Dassault Systèmes Biovia; 2016.
30. Berendsen HJ, van der Spoel D, van Drunen R. GROMACS: a message-passing parallel molecular dynamics implementation. Comput Phys Commun. 1995;91(1–3):43–56.
31. Huang J, MacKerell AD Jr. CHARMM36 all-atom additive protein force field: validation based on comparison to NMR data. J Comput Chem. 2013;34(25):2135–45.
32. Vanommeslaeghe K, et al. CHARMM general force field: a force field for drug-like molecules compatible with the CHARMM all-atom additive biological force fields. J Comput Chem. 2010;31(4):671–90.
33. Parrinello M, Rahman A. Polymorphic transitions in single crystals: a new molecular dynamics method. J Appl Phys. 1981;52(12):7182–90.
34. Van Tonder A, Joubert AM, Cromarty AD. Limitations of the 3-(4, 5-dimethylthiazol-2-yl)-2, 5-diphenyl-2H-tetrazolium bromide (MTT) assay when compared to three commonly used cell enumeration assays. BMC Res Notes. 2015;8:1–10.
35. Guo H, et al. Pomegranate (Punica granatum) extract and its polyphenols reduce the formation of methylglyoxal-DNA adducts and protect human keratinocytes against methylglyoxal-induced oxidative stress. J Funct Foods. 2021;83:104564.
36. Livak KJ, Schmittgen TD. Analysis of relative gene expression data using real-time quantitative PCR and the 2− ΔΔCT method. Methods. 2001;25(4):402–8.
37. Li Y, et al. Silencing of survivin expression leads to reduced proliferation and cell cycle arrest in cancer cells. J Cancer. 2015;6(11):1187.
38. Tomayko MM, Reynolds CP. Determination of subcutaneous tumor size in athymic (nude) mice. Cancer Chemother Pharmacol. 1989;24:148–54.
39. Tian J, et al. The antiproliferative and colony-suppressive activities of STAT3 inhibitors in human cancer cells is compromised under hypoxic conditions. Anticancer Res. 2017;37(2):547–53.
40. Guanizo AC, et al. STAT3: a multifaceted oncoprotein. Growth Factors. 2018;36(1–2):1–14.
41. Real PJ, et al. Resistance to chemotherapy via Stat3-dependent overexpression of Bcl-2 in metastatic breast cancer cells. Oncogene. 2002;21(50):7611–8.
42. Lee H, Jeong AJ, Ye S-K. Highlighted STAT3 as a potential drug target for cancer therapy. BMB Rep. 2019;52(7):415.
43. Wu L, et al. STAT3 exerts pro-tumor and anti-autophagy roles in cervical cancer. Diagn Pathol. 2022;17(1):1–10.
44. Ferraz E, et al. Investigation of the mutagenic and genotoxic activities of LLL-3, a STAT3 inhibitor. Drug Chem Toxicol. 2017;40(1):30–5.
45. Onimoe G-I, et al. Small molecules, LLL12 and FLLL32, inhibit STAT3 and exhibit potent growth suppressive activity in osteosarcoma cells and tumor growth in mice. Invest New Drugs. 2012;30:916–26.
46. Shao Z, et al. The Anticancer Effect of Napabucasin (BBI608), a natural naphthoquinone. Molecules. 2023;28(15):5678.
47. Kang J-H, et al. Inhibition of STAT3 signaling induces apoptosis and suppresses growth of lung cancer: good and bad. Lab Anim Res. 2019;35:1–9.
48. Redell MS, et al. Stat3 signaling in acute myeloid leukemia: ligand-dependent and-independent activation and induction of apoptosis by a novel small-molecule Stat3 inhibitor. Blood J Am Soc Hematol. 2011;117(21):5701–9.
49. Kong R, et al. Small molecule inhibitor C188–9 synergistically enhances the demethylated activity of low-dose 5-Aza-2′-deoxycytidine against pancreatic cancer. Front Oncol. 2020;10:612.
50. Jung KH, et al. Multifunctional effects of a small-molecule STAT3 inhibitor on NASH and hepatocellular carcinoma in mice. Clin Cancer Res. 2017;23(18):5537–46.
51. Tsimberidou AM, et al. Phase 1 trial evaluating TTI-101, a first-in-class, orally bioavailable, small molecule, inhibitor of STAT3, in patients with advanced solid tumors. J Clin Oncol. 2023;41:3018–8. https://doi.org/10.1200/JCO.2023.41.16_suppl.3018.
52. Bixel K, et al. Targeting STAT3 by HO3867 induces apoptosis in ovarian clear cell carcinoma. Int J Cancer. 2017;141(9):1856–66.
53. Li H, et al. Targeted activation of Stat3 in combination with paclitaxel results in increased apoptosis in epithelial ovarian cancer cells and a reduced tumour burden. Cell Prolif. 2020;53(1): e12719.
54. Qian S, et al. The role of BCL-2 family proteins in regulating apoptosis and cancer therapy. Front Oncol. 2022;12:985363.
55. Suvarna V, Singh V, Murahari M. Current overview on the clinical update of Bcl-2 anti-apoptotic inhibitors for cancer therapy. Eur J Pharmacol. 2019;862:172655.

56. Gómez-López S, Lerner RG, Petritsch C. Asymmetric cell division of stem and progenitor cells during homeostasis and cancer. Cell Mol Life Sci. 2014;71:575–97.
57. Wang Y, et al. Centrosome-associated regulators of the G 2/M checkpoint as targets for cancer therapy. Mol Cancer. 2009;8:1–13.
58. Nakamura H, et al. Therapeutic significance of targeting survivin in cervical cancer and possibility of combination therapy with TRAIL. Oncotarget. 2018;9(17):13451.
59. Kelly RJ, et al. Impacting tumor cell-fate by targeting the inhibitor of apoptosis protein survivin. Mol Cancer. 2011;10:1–11.
60. Chen X, et al. Survivin and tumorigenesis: molecular mechanisms and therapeutic strategies. J Cancer. 2016;7(3):314.
61. Li H-L, et al. A review of the regulatory mechanisms of N-myc on cell cycle. Molecules. 2023;28(3):1141.
62. Sun L, et al. Rapamycin targets STAT3 and impacts c-Myc to suppress tumor growth. Cell Chem biol. 2022;29(3):373-385. e6.
63. Zhang L, et al. Pharmacokinetics and pharmacodynamics of TTI-101, a STAT3 inhibitor that blocks muscle proteolysis in rats with chronic kidney disease. Am J Physiol-Renal Physiol. 2020;319(1):F84–92.

Publisher's Note